An Ensemble of Rapidly Interconverting Orientations in Electrostatic Protein–Peptide Complexes Characterized by NMR Spectroscopy

Jia-Ying Guan,[a] Johannes M. Foerster,[b] Jan W. Drijfhout,[c] Monika Timmer,[a] Anneloes Blok,[a] G. Matthias Ullmann,[b] and Marcellus Ubbink*[a]

Protein complex formation involves an encounter state in which the proteins are associated in a nonspecific manner and often stabilized by interactions between charged surface patches. Such patches are thought to bind in many different orientations with similar affinity. To obtain experimental evidence for the dynamics in encounter complexes, a model was created using the electron transfer protein plastocyanin and short charged peptides. Three plastocyanins with distinct surface charge distributions were studied. The experimental results from chemical shift perturbations, paramagnetic relaxation enhancement (PRE) NMR, and theoretical results from Monte Carlo simulations indicate the presence of multiple binding orientations that interconvert quickly and are dominated by long-range charge interactions. The PRE data also suggest the presence of highly transient orientations stabilized by short-range interactions.

Introduction

According to current models, formation of a specific protein complex is preceded by that of an encounter complex.[1] It is believed that, in this state, the partners assume multiple orientations to enhance the probability of finding the specific binding site.[2] Often in the encounter complex, charge–charge interactions dominate, whereas the specific (final) state is stabilized by various short-range interactions. The assumed presence of multiple orientations in the encounter state is based on the theoretical notion of charged surface patches. Like Velcro,[3] such patches can bind in many orientations with similar energy and thus all are assumed to be populated. The presence of multiple orientations and the dynamic exchange between them in the charge-driven encounter state is, however, not easy to demonstrate experimentally.

The aim of this study was to create a pure, charge-driven encounter state and demonstrate the existence of a rapidly changing set of binding orientations. We chose to study the complex of plastocyanin (Pc) and short, charged peptides (Lys$_4$), assuming that the interaction would be dominated by the strong positive charges of the peptides. The peptides are an artificial binding partner, so Pc will not have an optimized binding site, and a specific complex is unlikely to be formed.

Pc is a type I blue copper protein involved in the electron transport process in oxygenic photosynthesis, functioning as an electron carrier between cytochrome f (Cyt f) of the b_6f complex and P700$^+$ of photosystem I (PSI). Structures are available for Pc from various plants and bacteria.[4–11] One of the histidine residues that is a copper ligand is considered to be the electron entrance, that is, it provides a strong coupling pathway toward the copper. It is located at the so-called "northern" side of the protein, within a hydrophobic patch. Pc is acidic in higher plants[5,9–12] and green algae,[13–15] possessing two highly conserved negatively charged surface regions (acidic patches) formed by amino acids at positions 42–44 and 59–61 on the so-called "eastern" side. A typical example of *Populus nigra* Pc (PoPc) is shown in Figure 1 A. Compared to typical plant Pcs, the structure of Pc from the fern *Dryopteris crassirhizoma* (DPc) has the same global structure (Figure 1 B), but a large acidic arc extends to the northern side surface near the hydrophobic patch, resulting in distinct electrostatic properties.[7] In cyanobacteria, Pc can also be almost neutral[6,16] such as in *Phormidium laminosum*[6] (Figure 1 C), or basic, such as in *Nostoc* sp. PCC 7119.[17–19]

Charged peptides have proved useful for studying interacting sites in electron transfer proteins, including Pc, Cyt f, and Cyt c.[20–26] Experimental results showed that positively charged polylysine peptides interact with the clustered acidic residues on Pc and competitively inhibit electron transfer from Cyt c or Cyt f to Pc.[20,22] This competitive inhibition was explained by neutralization of charges by the formation of the Pc–peptide complexes.[20] The binding of polylysine peptides to Pc can also subtly perturb the active-site geometry and the redox potential.[20,23] Little information, however, is available for the

[a] Dr. J.-Y. Guan, Dr. M. Timmer, A. Blok, Prof. Dr. M. Ubbink
Leiden Institute of Chemistry, Gorlaeus Laboratories, Leiden University
Einsteinweg 55, 2333 CC Leiden (The Netherlands)
E-mail: m.ubbink@chem.leidenuniv.nl

[b] J. M. Foerster, Prof. Dr. G. M. Ullmann
Structural Biology/Bioinformatics, University of Bayreuth
Universitätsstrasse 30, 95447 Bayreuth (Germany)

[c] Dr. J. W. Drijfhout
Department of Immunohematology and Blood Transfusion
Leiden University Medical Center
Albinusdreef 2, 2333 ZA Leiden (The Netherlands)

Supporting information for this article is available on the WWW under
http://dx.doi.org/10.1002/cbic.201300623.
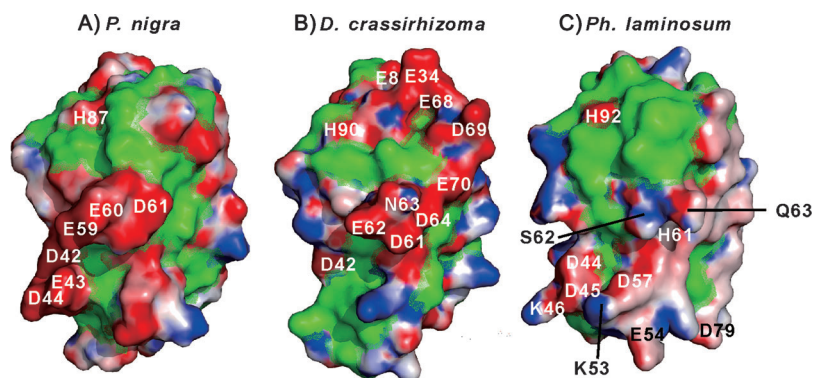
Figure 1. Electrostatic potential maps of Pc surface models (PDB IDs: 1TKW,[32] 1KDI,[7] and 2Q5B). The surface colors correspond to the electrostatic potential calculated by the program APBS[63] at an ionic strength of 10 mM, pH 6.5, 300 K, to match the experimental conditions. The electrostatic potentials are colored and contoured from −8 (intense red) to +8 kT/e (intense blue). Hydrophobic residues (Ala, Val, Ile, Leu, Phe, Pro, Tyr, and Met) are colored in green. Several relevant residues are labeled. Pictures were generated using PyMOL.[64]

binding interface and the underlying degree of dynamics in the interaction.

Paramagnetic relaxation enhancement (PRE) NMR spectroscopy has been used as a sensitive tool to detect lowly populated intermediates in biomolecular complexes.[27,28] The large magnetic moment of the unpaired electron from the paramagnetic center causes relaxation of nuclear spins in the vicinity. This effect diminishes very rapidly, being proportional to the inverse sixth power of the distance between the electron and the nucleus. TOAC (2,2,6,6-tetramethyl-N-oxyl-4-amino-4-carboxylic acid) has been shown to be useful for PRE NMR studies of protein–peptide interactions.[29] One of the advantages of TOAC over side chain-attached spin labels is that TOAC can be directly incorporated into the peptide backbone in automated peptide synthesis. There has been growing interest in using TOAC in peptide–protein and peptide–nucleic acid interactions and in combination with other physical techniques, such as electron paramagnetic resonance (EPR), circular dichroism (CD), fluorescence, Fourier-transform infrared (FT-IR), NMR, and X-ray crystallography, to understand molecular interactions.[30]

In this study, the transient complexes formed by tetralysine peptides and three different Pcs were studied using chemical shift perturbation (CSP) analysis, PRE NMR spectroscopy, ensemble docking, and Monte Carlo (MC) simulations. The CSP data corresponded well with the electrostatic MC docking calculations, clearly showing that binding is dominated by charge interactions. The PRE data indicated that, within the electrostatic ensemble, the peptides assume multiple orientations in a dynamic fashion. The PRE data also provide evidence for the presence of orientations that are slightly more favored than expected from pure charge–charge interactions, perhaps due to transient hydrogen bond formation with TOAC or weak hydrophobic interactions. Overall, the experimental and simulation results provide direct evidence for dynamics in an encounter complex dominated by charge–charge interactions.

Results

Backbone assignments

To study the three Pcs by NMR, the proteins were isotopically labeled with ^{15}N for PRE measurements and ^{15}N/^{13}C for resonance assignments. To eliminate the paramagnetic effect of Cu^{2+}, Zn-substituted Pc was used. For DPc and PoPc, backbone amide resonances were assigned by using HNCACB experiments on ^{13}C/^{15}N-labeled proteins. The assignments of Cu^I-DPc (BMRB code 7370)[31] and Cu^I-PoPc (BMRB code 4019) were used as the starting points. Data for backbone assignments (H, N, C_α, C_β) have been deposited to BMRB under codes 19236 (DPc) and 19247 (PoPc). Assignments of Zn-substituted PhPc were kindly provided by Dr. Sandra Scanu (Leiden University). For DPc, the resonance of Ser92 was not found in the spectra. For PoPc, some residues close to the N terminus have double peaks. These double resonances exist for Ile1, Asp2, Val3, Ser20, Ile21, Ser22, Pro23, Gly24, Glu25, Lys26, Ile27, Val28, Lys30, Met57, Thr69, Phe70, Glu71, Val72, Leu74, and Gly78. Similar observations were described for Cd-PoPc.[32] The double signals were attributed to partial processing of the N-terminal methionine in the bacterial cytoplasm, as these residues are located near the N terminus in the three-dimensional structure of the protein.[32]

Chemical shift perturbations

To study the interaction of Pc with lysine peptides, four types of peptides were used. For the PRE experiment described below, a TOAC residue (X) was introduced at the N or C terminus (X-Lys$_4$ and Lys$_4$-X). As controls for the introduction of TOAC, Ala-Lys$_4$ and Lys$_4$-Ala were also used. First, the interactions of these peptides with the three Pc variants were studied using CSP analysis.

Each ^{15}N-Pc was titrated with the four peptides individually in a low ionic strength buffer ($I = 10$ mM), and ^{1}H,^{15}N HSQC spectra were acquired at each titration point. For these studies, TOAC was reduced to eliminate its paramagnetic effects. Addition of the peptides gave rise to small CSPs in the ^{1}H,^{15}N HSQC spectra of all Pcs, with maximum observed average shifts ($|\Delta\delta_{ave}|$) of 0.07 ppm for PoPc, 0.05 ppm for DPc, and 0.01 ppm for PhPc (Figure 2). Single, averaged resonances were observed for all amides, indicating fast exchange between the free and bound Pc on the NMR time scale. Binding maps, obtained by coloring the protein residues according to the size of CSP, show similar patterns for different peptides for the same Pc (Figure 2 for Lys$_4$-X and Figure S1 for the other peptides). The similar patterns observed for Lys$_4$-X and X-Lys$_4$ indicate that
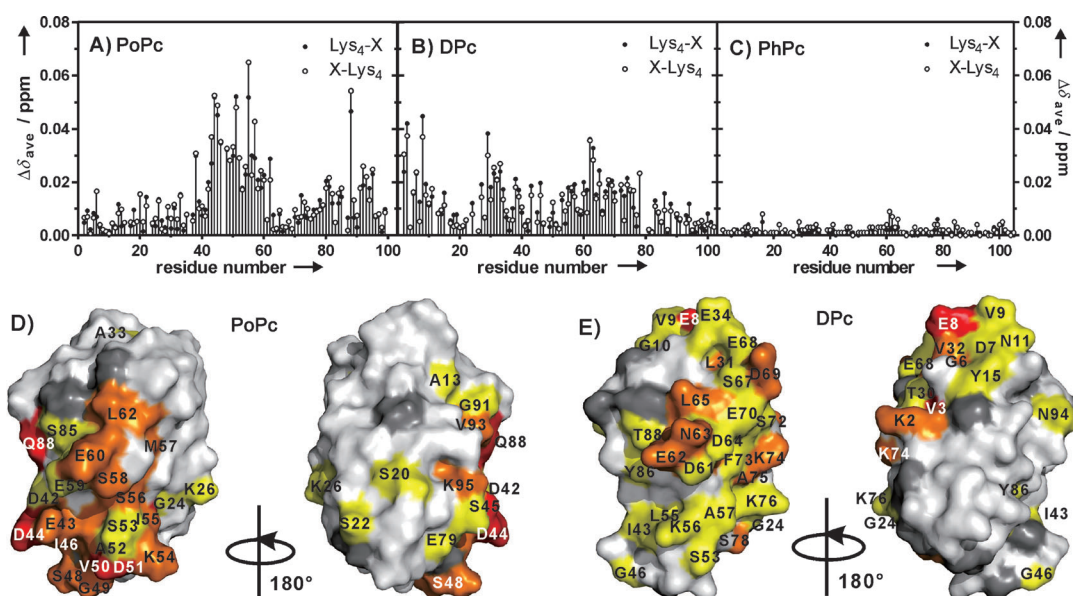
Figure 2. A)–C) Plots of NMR chemical shift perturbations measured for Pc backbone amides in the presence of TOAC-containing peptides. Extrapolated values (to 100% bound) for PoPc and DPc, and observed values for PhPc, are shown. D) and E) CSPs (extrapolated to 100% bound, see Table 1 for bound fractions) mapped onto the protein surfaces from the binding of Lys$_4$-X to PoPc (panel D, PDB ID: 1TKW[32]) and DPc (panel E, PDB ID: 1KDI[7]). Red, $\Delta\delta_{ave} \geq$ 0.04 ppm; orange, $0.04 > \Delta\delta_{ave} \geq 0.02$ ppm; yellow, $0.02 > \Delta\delta_{ave} \geq 0.01$ ppm; white, $\Delta\delta_{ave} < 0.01$ ppm; Gray, no data or overlapping resonances. Binding maps for the other peptides are shown in Figure S1.

the CSPs are caused by interactions with the four lysines. The binding maps of Ala-Lys$_4$ and Lys$_4$-Ala were also similar to those of X-Lys$_4$ and Lys$_4$-X, indicating no significant effect of TOAC on peptide binding (Figure S1).

In PoPc and DPc, most CSPs occurred around the regions with the acidic patches, in agreement with the assumption that the positively charged peptides interact with the acidic residues of Pc.[20, 33] The largest CSPs for PoPc occurred for residues Asp44, Ser45, Asp51, Ile55, and Gln88. Among these residues, Asp44 belongs to the acidic patch. For DPc, the largest CSPs occurred for residues Val3 and Glu8. Glu8 is located at the acidic arc on the northern side. Although the observed CSPs are very small for PhPc, similar effects were still observed from both TOAC-containing peptides (Figure 2C). The small perturbations of the resonances of the copper ligand residues (His37, Cys84, His87, and Met92 for PoPc; His37, Cys87, His90, and Met95 for DPc; His39, Cys89, His92, and Met97 for PhPc) indicate that the copper site is not the main binding site of the peptides. Similar magnitudes of perturbations and binding maps caused by a tetralysine peptide (without an additional TOAC) were observed for Pc from the seed plant *Silene pratensis*.[34]

Binding constants were obtained by fitting the CSP curves for the most affected residues (Figure 3, Figures S2 and S3, and Table 1). For PhPc, the magnitudes of the observed CSPs were too small ($|\Delta\delta_H| \leq 0.01$ ppm) to determine a dissociation constant.

The binding curves for PoPc fitted well to a single binding site model (Figure 3A). Interestingly, there were two types of dissociation constants observed in DPc titrations. The residues that are involved in stronger binding (lower K_d) were clustered on the northern side of DPc (Figure 2E and Figure S3B). This might be due to the unusual surface charge distribution of DPc compared with other plant Pcs. It is possible that there is internal competition between the two binding sites for the peptides. Clearly, a 1:1 binding model is not appropriate to explain this observation. Therefore, a two-site binding model was used to obtain the K_d values for DPc (Figure 3B and C, Figure S2B and C, and Figure S3C–F).

For most peptides, the K_d values for the same Pc are similar, indicating that the TOAC caused no significant changes in the affinity of the peptides for Pc. Only Lys$_4$-X has a somewhat lower K_d for PoPc than Lys$_4$-Ala, but the difference is within the error margins.

Table 1. Dissociation constants of the complexes formed between Pc(Zn) and tetralysine peptides and their calculated bound fractions at the end point of the titrations.

Pc	Lys$_4$-Ala		Lys$_4$-X		Ala-Lys$_4$		X-Lys$_4$	
	K_d [µM]	Fraction	K_d [µM]	Fraction	K_d [µM]	Fraction	K_d [µM]	Fraction
PoPc	150 ± 40	0.95	90 ± 30	0.97	110 ± 20	0.97	130 ± 40	0.96
DPc (strong)	110 ± 20	0.97	110 ± 20	0.97	110 ± 20	0.98	110 ± 20	0.96
DPc (weak)	300 ± 40	0.91	300 ± 50	0.90	340 ± 40	0.94	300 ± 100	0.94

A)

B)

C)
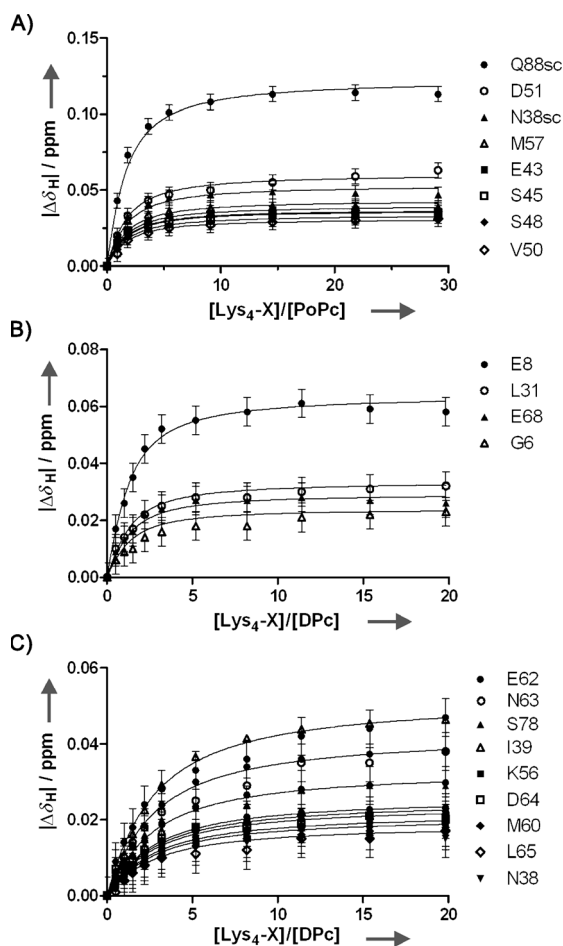
Figure 3. Chemical shift changes of selected Pcs resonances as a function of increasing [peptide]/[Pc]. The dissociation constants of the corresponding peptides (Table 1) were obtained by simultaneous fitting to a 1:1 binding model for PoPc (solid lines) and by simulation of two-site binding for DPc. Error bars represent ±0.005 ppm. A) Lys$_4$-X with PoPc; B) Lys$_4$-X with DPc, strong binding residues; C) Lys$_4$-X with DPc, weak binding residues.

Paramagnetic relaxation enhancements

The paramagnetic TOAC was introduced to determine whether the bound peptide possesses a single, well-defined orientation or several orientations. If the peptide orientation is well-defined, the strong distance dependence of the PRE should result in highly localized effects. The TOAC was placed at the N or C terminus of the tetralysine peptide in order to interfere minimally with binding.[29] The attached spin labels were thus expected to yield PRE of nuclei on nearby Pc residues. If the peptides bind in a specific orientation, the N- and C-terminal TOACS should generate different PRE patterns.

PREs were observed for some residues, as shown in Figure 4. Binding of these peptides to the three Pcs is in the fast-exchange regime, so the observed PRE is a weighted average of free Pc (no PRE) and bound Pc. By dividing the observed PRE by the fractions bound, calculated from the K_d, the PRE for 100% bound Pc was obtained. For DPc, the weak-binding K_d values were used, because most residues showed weak binding.

For PoPc binding to Lys$_4$-X, the resonances that were broadened beyond detection were those of Gly49, Glu59, and the side chain of Gln88. For PoPc binding with X-Lys$_4$, the resonance of an additional residue (Glu43) was completely broadened. These residues are located on the same side as the acidic patches, which include Glu43 and Glu59. Resonances of many residues located around the acidic patch also experienced PRE at various magnitudes. This observation indicates that the binding sites of the peptides on Pc are not restricted to the acidic patch residues only, but also extend to other polar or charged residues around this region and even to the hydrophobic patch, including some positive residues such as Lys26, Lys54, and Lys66 (I_{para}/I_{dia} ratio: 0.60–0.84). This observation suggests that the peptides sample a large area of the protein surface and demonstrates the superior sensitivity of PRE for transient interactions.

For the interaction of DPc with Lys$_4$-X and X-Lys$_4$, the resonances of three residues disappeared from the spectra: Gly33, Gly36, and Glu68. Resonances of two other acidic residues (Glu34 and Asp69) were broadened but still visible in the spectra (I_{para}/I_{dia} ratio: 0.59–0.82). These five residues are close together on the acidic arc at the northern side of DPc, indicating that the cluster of negative charges on the protein attracted the peptides by charge–charge interactions.

For PhPc, only one resonance (Thr75) had a clearly significant PRE (I_{para}/I_{dia} ratio: 0.5) under the experimental conditions (peptide/protein ratio: 1:1). The I_{para}/I_{dia} ratios of Val48, Leu55, His61 and Gln63 were 0.84, 0.83, 0.84, and 0.83, respectively. These values are close to the defined threshold for unaffected residues (I_{para}/I_{dia} ratio: 0.85).

The PRE effects of tetralysine peptides on DPc are smaller than on PoPc in general. This is due to a smaller bound fraction. The nuclei that experience the largest CSP in DPc are not those that exhibit the largest PRE, probably because CSP monitors the effects from all atoms within the peptides, whereas PRE indicates the effects from the paramagnetic center only.

It is interesting to note that strongly affected residues have unaffected neighbors. One such example is Ala73 of PoPc, which is affected by PRE, while the neighboring Val72 and Leu74 are not. Similarly, Ala75 of DPc, located in between the residues with PREs (Lys74 and Lys76), remains unaffected. Another example is seen with Asp61 and Glu62 of DPc, both located on the acidic arc. Asp61 is affected, but Glu62 is unaffected. These findings suggest highly localized effects and will be discussed in more detail later.

Ensemble docking

Visualization of the encounter state on the basis of PRE data can be carried out quantitatively by using the ensemble docking approach.[28] Calculations were performed using 1–15 copies of a pseudoatom that represents the paramagnetic center. Experimental PREs were converted into distances for ensemble docking. For DPc, the K_d values used here are the low affinity values, as most residues belong to the low affinity group. The high affinity residues were completely broadened; therefore, their target distance ranges are the same using
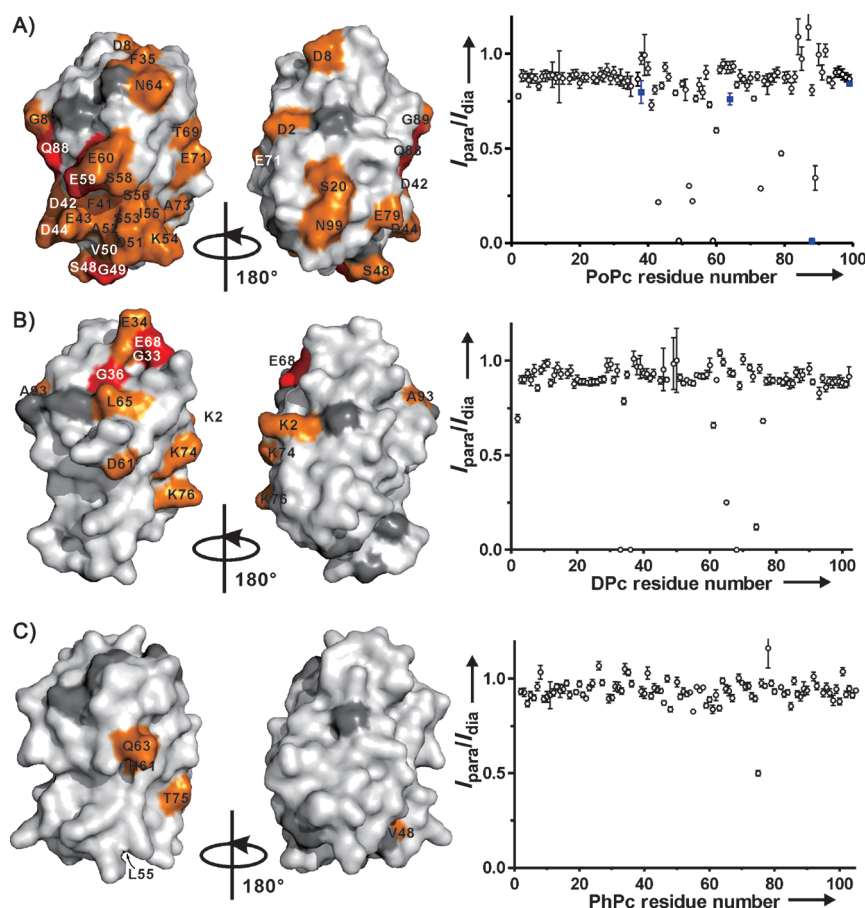
Figure 4. PRE effects in Pc–Lys$_4$-X complexes. The paramagnetic peptide was added to Pc at a peptide/Pc molar ratio of 0.5 for DPc and 1 for PoPc and PhPc, resulting in fractions of bound Pc of 14% for DPc and 35% for PoPc. The bound fraction for PhPc is unknown but expected to be very small. Left: A) PRE maps of PoPc (PDB ID: 1TKW[32]), B) DPc (PDB ID: 1KDI[7]), and C) PhPc (PDB ID: 2Q5B) bound to the Lys$_4$-X peptide. Surface model colors: red, $I_{para}/I_{dia} < 0.1$; orange, $0.1 \leq I_{para}/I_{dia} < 0.85$; white, $I_{para}/I_{dia} \geq 0.85$; gray, prolines, unassigned, and overlapping resonances. Right: relative ^{1}H,^{15}N HSQC intensities of the backbone amide of A) PoPc (including side chains, which are shown as blue squares), B) DPc, and C) PhPc in complex with TOAC-containing peptides. Error bars denote twofold standard deviations, derived from spectral noise levels using standard error propagation procedures. For most data points, the error bars are within the symbol.
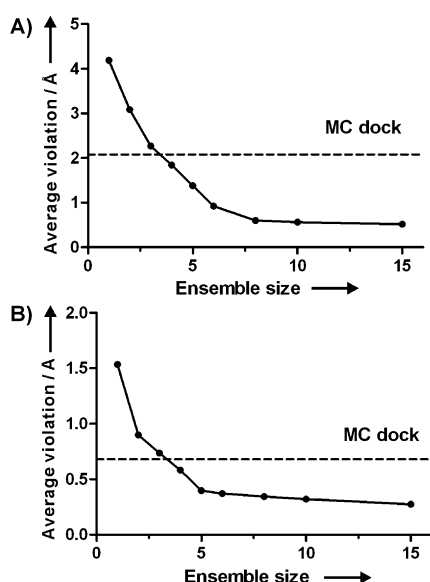
spends a short time being very close to the affected amide. Most of the affected amides have a considerable accessible surface area (ASA), which enables a close contact with the TOAC. In general, no major differences were observed for X-Lys$_4$ and Lys$_4$-X.

Monte Carlo simulations

Previous studies have shown that many encounter complexes are predominantly stabilized by electrostatic forces,[2] although in some cases, short-range hydrophobic interactions may also contribute.[35] Visualization of the encounter complex of Cyt c and Cyt c peroxidase was successfully achieved using PRE data and rigid-body MC simulations.[36] The results showed that formation of this encounter complex was driven by charge–charge interactions. In MC simulations, one protein is docked to the other, guided by an electrostatic field and MC sampling.[37] In this way, charge–charge interactions represent the only force that brings the binding partners together. Rigid-body MC docking simulations were performed for the Pc–peptide complexes, and a Boltzmann distribution of orientations of the peptide in complex with Pc was obtained. The paramagnetic centers of the peptides in this distribution are shown as green (Lys$_4$-X) and blue (X-Lys$_4$) spheres around Pc in Figure 7.
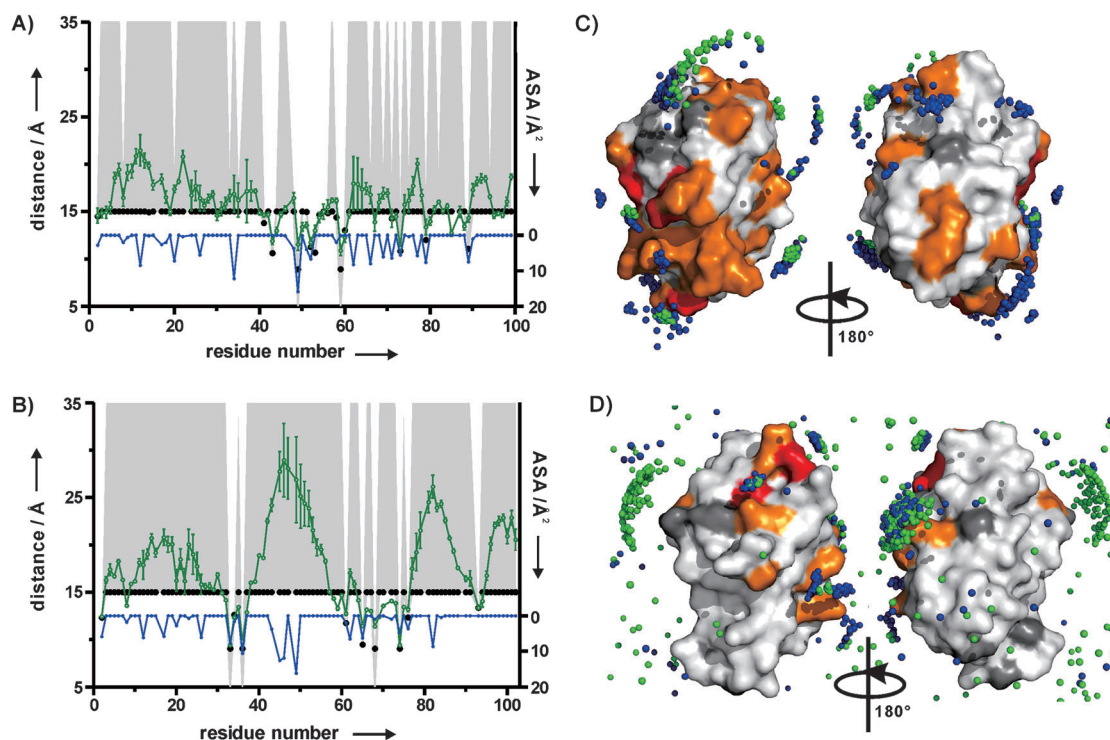
The results for PoPc (Figure 7 A) and DPc (Figure 7 B) show that the peptides are located close to the acidic patches. For PhPc, the population is more randomly distributed, with a relatively higher density at the side of PhPc that is farthest from the hydrophobic patch (Figure 7 C).

The distances from the nitroxy oxygen of the TOAC to the Pc amide hydrogens were measured and averaged (using r^{-6} averaging) for an ensemble existing of 2000 orientations randomly selected from the entire distribution. The distances obtained were compared with the experimental values. The violations calculated for the MC docking ensemble were 2.08, 1.70, 0.68, and 0.56 for PoPc–Lys$_4$-X, PoPc–X-Lys$_4$, DPc–Lys$_4$-X, and DPc–X-Lys$_4$, respectively. All violations are in the middle of the range of values shown in Figure 5 A and B and Figure S5 A and B). Thus, the MC docking ensemble does not fully agree with the PRE data. Figure 8 shows the back-calculated average dis-

either K_d value. Violations were defined as the absolute differences between the distance back-calculated from the entire ensemble (by using r^{-6} averaging) and the experimental distance. Figure 5 shows the results of ensemble docking for Lys$_4$-X binding to PoPc and DPc with increasing ensemble size. Large distance violations occurred when using a single representation of the paramagnetic center (Figure 5, $N = 1$), indicating that multiple orientations are required to describe the data. As a result of increasing degrees of freedom, the distance violations were reduced with increasingly larger ensembles. For PoPc (Figure 5 A), no significant reduction in violation occurred at $N \geq 8$. For DPc, the violation curve flattened at $N = 5$ (Figure 5 B).

The resulting ensembles for $N = 6$ are shown in Figure 6. Most of the paramagnetic centers are located in well-defined positions and not in a "cloud" of orientations. This correlates with the observation that some amides of Pc are strongly affected by PRE, whereas others that are nearby are not. That can be explained by assuming that the paramagnetic center

Figure 5. Averaged distance violations against a number of paramagnetic pseudoatoms ($N = 1$–6, 8, 10, 15) in the ensemble docking. A) Lys$_4$-X–PoPc, B) Lys$_4$-X–DPc. The dashed horizontal lines indicate the average violations calculated from MC dock.

tances for each Pc residue in comparison with the PRE-derived distances. Although MC docking clearly places the paramagnetic center close to the affected residues, the simulation underestimates the PRE for these residues.

Figure 9 shows the plots of electrostatic interaction energy distribution for the Pc–Lys$_4$-X complexes. PoPc (Figure 9 A) and DPc (Figure 9 B) have similar patterns. The highest population in DPc was at -6 kcal mol^{-1}, whereas in PoPc it was at -7 kcal mol^{-1}. For PhPc (Figure 9 C), it is clear that the charge–charge interaction is much weaker (highest population at -2 kcal mol^{-1}). Histograms for the Pc-X-Lys$_4$ complexes are shown in Figure S5. The highest populations appeared at -8, -7, and -2 kcal mol^{-1} for PoPc, DPc, and PhPc, respectively.

Discussion

The aim of the present work was to experimentally characterize the dynamics in encounter complexes. The rationale was to create a pure encounter complex by ensuring that electrostatics dominate the interactions. For this purpose, the complexes formed by charged tetralysine peptides and three Pcs with distinct surface charge properties were studied. At pH 6.5, the net charges of PoPc, DPc, and PhPc are -7, -5, and -1, respectively, and the charge distributions differ markedly between these Pcs.

Previously, the interaction between the seed plant *S. pratensis* Pc and lysine peptides of varying lengths was studied using circular dichroism, UV–visible absorption, resonance Raman spectroscopy, and cyclic voltammetry. Minor changes in the geometry of the copper site were observed upon peptide binding.[20, 23] The peptides also competitively inhibited electron
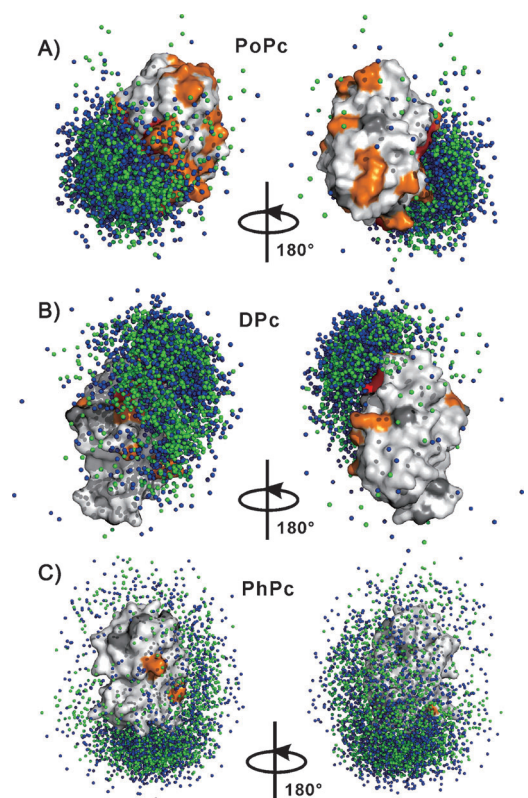

Figure 6. Ensemble docking. A) and B) Correlation of experimental distances (black dots) and back-calculated average distances (green dots with green connecting lines) from the ensemble docking ($N = 6$, 20 lowest energy structures) of Lys$_4$-X bound to A) PoPc and B) DPc, with error bars representing the standard deviation. Right y-axes indicate the accessible surface area (ASA) of each amide proton, shown as blue dots with blue connecting lines. Gray areas indicate the error margins of the experimental distances. C) and D) PRE-based ensemble docking results ($N = 6$) of C) PoPc (396 solutions for Lys$_4$-X and 594 for X-Lys$_4$) and D) DPc (630 solutions for Lys$_4$-X and 360 for X-Lys$_4$). The paramagnetic centers from TOAC are shown as spheres, with Lys$_4$-X in green and X-Lys$_4$ in blue. Protein surfaces are colored the same as in PRE maps (Figure 4).

Figure 7. MC docking results showing 2000 solutions of Lys$_4$-X and X-Lys$_4$ bound to A) PoPc, B) DPc, and C) PhPc. The paramagnetic centers of the peptides are shown as green (Lys$_4$-X) and blue (X-Lys$_4$) spheres. Protein surfaces are colored according to the PRE maps (Figure 4). The 2000 orientations in each ensemble were selected randomly for the entire MC docking solution set.
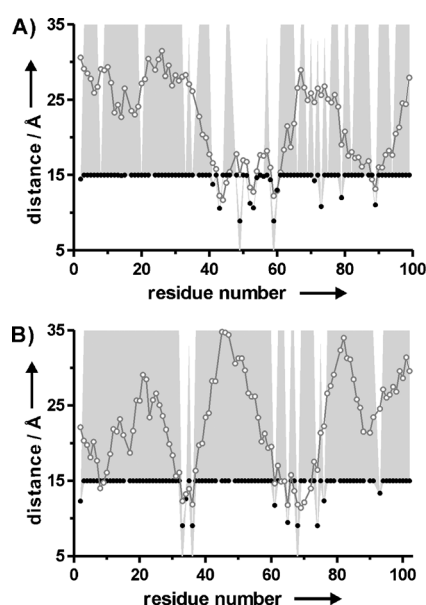
Figure 8. Comparison of experimental distances (dots) and back-calculated average distances (circles with connecting lines) between Pc amides and the TOAC nitroxy oxygen atoms in the ensembles from MC simulations (2000 structures). A) PoPc–Lys$_4$-X; B) DPc–Lys$_4$-X.
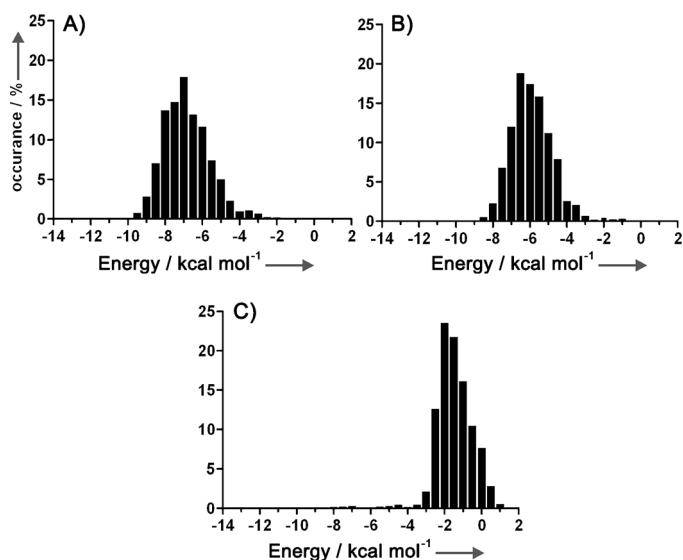
Figure 9. Histograms showing the electrostatic interaction energy distribution of 2000 structures randomly selected from the MC simulations. A) PoPc–Lys$_4$-X, B) DPc–Lys$_4$-X, C) PhPc–Lys$_4$-X.

transfer from Cyt f[22] and Cyt c.[20] Mutagenesis of Pc showed that the interaction and electron-transfer inhibition by lysine peptides decreased significantly as the net charge of the Pc negative patch decreased,[20] showing that charge interaction contributed to the binding. The authors of this study proposed a specific and effective interaction between the positively charged peptides and the negative patches of Pc.[20] These studies monitored spectroscopic changes caused by peptide binding but could not directly observe the binding interface and the dynamics of the interaction. Other studies of highly charged electron transfer proteins with small- or medium-sized molecules also emphasized the importance of charge–charge interactions in binding. Increasingly tight binding to Cyt c was observed for porphyrins with an increasing number of carboxylates, even with subnanomolar K_d values.[38,39] Structural characterization of the complex of Cyt c with similar, though more weakly binding porphyrins (high micromolar range) by CSP analysis suggested mobility of the porphyrin on the protein surface.[40] Cyt c has also been shown to interact with calixarenes. When decorated with many negative charges, these compounds compete effectively with natural protein partners for binding to Cyt c.[41] A recent and elegant structural study showed that calixarenes interact with several amino groups of lysines, taking several specific conformations on the surface of the cytochrome.[42]

Charge–charge interactions

To establish whether charge–charge interactions were the dominating interaction force in the Pc–Lys$_4$ complexes, the interaction surface was mapped using CSPs and compared with the results from the electrostatically driven MC simulations. In PoPc and DPc, CSPs were largest in the acidic regions. The K_d values were about 100 μM for PoPc and 110 μM and 300 μM for the two binding sites on DPc. For PhPc, peptide binding re-

sulted in very small CSPs, suggesting a low affinity. No dissociation constant could be determined. These results are in good agreement with the MC simulations. The electrostatic ensembles match well with the CSP-derived binding maps for PoPc and DPc. The electrostatic interaction energies indicated that these two Pcs have a strong interaction, whereas for PhPc, the affinity was quite weak. The data indicate that charge-driven binding is a good first description of the complexes.

Paramagnetic relaxation effects

To determine whether the peptides assume a single, well-defined orientation or exhibit multiple orientations, the paramagnetic amino acid TOAC was incorporated at the N or C terminus of tetralysine peptides. Control peptides with Ala instead of TOAC were used to assess the effect of TOAC incorporation on peptide binding to Pc. No significant difference between the binding affinities of TOAC- and Ala-tetralysine peptides was observed, indicating that TOAC has little influence on the thermodynamics of peptide binding.

In PoPc, the presence of TOAC caused PREs mainly in the neighborhood of the acidic patches as well as for some of the hydrophobic patch residues. Almost no CSPs were observed in the hydrophobic patch, which suggests that the PREs for those residues represent peptide orientations that are sparsely populated. The PRE is highly sensitive for minor states in which the paramagnetic center is brought within close proximity of the nucleus. Apparently, transiently peptide–protein interactions that are not dominated by electrostatic forces were present. In DPc, the area affected by PREs is smaller and more localized than in PoPc. The largest PREs were detected around the top of the acidic arc, close to the copper site. The PRE and CSP maps were similar in this case. For PhPc, few PREs and CSPs were observed, in accordance with the weak affinity for tetralysine peptides.

Dynamics in the complexes

It is believed that the overall size of the CSP is a measure for the degree of dynamics in a protein complex. Large CSPs are caused by a single, well-defined orientation in the complex, in which desolvation of the interface and multiple short-range interactions occur. Small CSPs indicate averaging of multiple orientations in the encounter state, with minimal desolvation. Small CSPs have been observed in several complexes of redox proteins that are thought to be highly dynamic, including Cyt b_5–myoglobin,[48] Cyt c–adrenodoxin,[49] Cyt c–Pc,[50] and Cyt c–Cyt b_5.[51] In this study, similarly small CSPs were observed in all Pc–peptide complexes. Small CSPs can be caused by a dynamic interaction or simply low affinity. In the case of PoPc and DPc, the CSPs could be extrapolated to 100% on the basis of the K_d value, demonstrating that the CSPs are indeed small for the fully bound Pc. For PhPc the CSPs were too small even to derive a reliable K_d value. To support the hypothesis that small overall CSP values correlate with dynamic interactions, we used PRE mapping. The observed PREs were scattered over the Pc surface, and both for PoPc and DPc, they could not be satisfied by a single orientation of the peptides. Furthermore, the N- and C-terminal TOAC-containing peptides gave very similar PRE maps, which is not to expected for peptides binding in well-defined orientations. Thus, qualitatively, the PRE results strongly support a dynamic binding model in which the peptide assumes many orientations relative to Pc and interconverts between these orientations faster than the NMR time-scale defined by the maximum CSP (exchange rate $\gg 250\ s^{-1}$).

Back-calculated distances using the ensemble docking approach with multiple orientations showed a good correlation with the experimental PREs for ensemble sizes much larger than 1, which is in line with dynamics within the complex. Also, the average distances between TOAC and Pc amides of the MC docking ensembles matched the experimental distances qualitatively but not quantitatively; the TOAC molecules were, on average, not close enough to the affected Pc amide groups to explain the observed PREs. This observation could be a consequence of the limitations of the docking method, such as the use of an exclusion grid to avoid steric hindrance. Alternatively, it could point toward small contributions of interactions other than electrostatics, perhaps very transient hydrogen bond formation between the exposed amide protons and the oxygen of TOAC. Evidence for the latter explanation comes from the PRE pattern. It is remarkable that the NMR resonances of several residues were broadened beyond detection due to a PRE, whereas those of neighboring amides were (almost) unaffected. The distance between neighboring amides is about 4 Å, so the PRE ratio for two amide residues is at most proportional to $r^{-6}/(r+4)^{-6}$, where r is the distance between the nitroxy radical and the nearest amide proton. It can be shown that, at least for some amides, this must imply that the TOAC nitroxy group approaches very closely, within several Ångströms for a short fraction of the time, which suggests that the sensitivity of PRE for minor states provides evidence for weak and transient short-range interactions. In physiological systems of protein–protein complexes such interactions must occur in the encounter complex next to the dominant charge–charge interactions for the complex to proceed to the final, well-defined complex.

Conclusions

The binding of tetralysine peptides to Pcs with different surface charge properties was characterized by a combination of CSP, PRE NMR, and MC simulations. The high similarity of CSP maps for the different peptides used in the study, as well as the small magnitudes of CSPs, strongly suggests a high degree of dynamics. Also, the scattered distribution of PREs indicates the presence of multiple orientations. The peculiar distribution of peptide positions obtained from ensemble docking with high densities in small areas only qualitatively matches the electrostatic docking simulations, suggesting that the PRE approach picks up very transient, short-range interactions between the peptide and the protein, in which the TOAC closely approaches specific amide protons.

Experimental Section

Peptide synthesis and preparation: Fmoc-TOAC-OH was purchased from Iris Biotech (Germany). Synthetic peptides Ala-Lys$_4$, Lys$_4$-Ala, TOAC-Lys$_4$ (X-Lys$_4$), and Lys$_4$-TOAC (Lys$_4$-X) were prepared as described,[29] with N-terminal acetylation and C-terminal amidation. Peptide purity was verified by rpHPLC, and peptide integrity was assessed by MALDI-TOF mass spectrometry. The peptides were dissolved in 10 mM NaPi, pH 6.5. The fraction of paramagnetic peptide was checked by EPR and found to be close to 100%. The quantity of trifluoroacetic acid (TFA) in the samples was confirmed by ^{19}F NMR with trifluorotoluene as the internal reference. A TFA/peptide molar ratio 5:1 was used to calculate the peptide concentration.

Protein expression and purification

General procedure: ^{15}N-enriched M9 minimal media was prepared as described previously.[52] For PoPc and PhPc, copper was excluded during bacterial growth. For additional ^{13}C labeling, the minimal medium was supplemented with 2 g L^{-1} ^{13}C-glucose. Cells were harvested by centrifugation and lysed with a French pressure cell (Stansted Fluid Power Ltd.) in the presence of 1 mg lysozyme, 3.75 mg DNase, 1 mM PMSF, and ZnCl$_2$ (100 μM for PoPc and DPc, 5 mM for PhPc). For PoPc and DPc, an additional 250 μM of ZnCl$_2$ was added after passing through the French press. Cell debris was removed by centrifugation at 7000 g for 25 min, and membranes were removed by ultracentrifugation at 25 000 g for 1 h. All columns used for purification were purchased from GE Healthcare Biosciences. PoPc and DPc concentrations were determined using the Bradford assay (Bio-Rad) with bovine serum albumin as the standard. Pc was considered pure when the protein migrated as a single band on SDS-PAGE (15%, 200 V, 50 min).

PoPc: The PoPc gene from plasmid pETPc[32] was subcloned into a pET28 plasmid with an additional glycine residue at the N terminus. ^{15}N-labeled PoPc was essentially produced as described[32] with the following modification: the protein was expressed in *E. coli* (Rosetta 2) in M9 minimal medium (1 L, 0.5 L per 2 L Erlenmeyer flask). Protein production was induced by adding IPTG to a final concentration of 0.5 mM. Incubation was continued at 16 °C overnight. The protein was purified using 3×5 mL HiTrap-DEAE FF ion-exchange columns in 20 mM sodium phosphate, pH 7.0. The protein was eluted with a gradient of 0–500 mM NaCl. Fractions containing PoPc were concentrated and purified by a Superdex G-75 size-exclusion column in 20 mM sodium phosphate, pH 6.8, 100 mM NaCl. The yield of pure protein was 1.5 mg L^{-1} of culture for ^{15}N-PoPc and 0.75 mg L^{-1} of culture for ^{15}N,[13]C-PoPc.

DPc: [15]N- and ^{15}N/^{13}C-labelled recombinant DPc containing zinc was produced in *E. coli* BL21(DE3) and purified as described before[31] with the following modifications: all copper salts were replaced by ZnCl$_2$ during purification. The protein was purified using 3×5 mL HiTrap-Q HP ion-exchange columns in 10 mM sodium phosphate, pH 5.8 at 4 °C. The impurities were eluted with a gradient of 0–100 mM NaCl at 4 mL min^{-1}, and the Pc protein was eluted in 100 mM NaCl at 0.5 mL min^{-1}. Then, size-exclusion chromatography with a Superdex G-75 column was performed in a buffer of 10 mM sodium phosphate, pH 6.5 and 100 mM NaCl. The yield of pure protein was 149 mg L^{-1} of culture for ^{15}N-DPc and 19 mg L^{-1} of culture for ^{15}N,[13]C-DPc.

PhPc: Uniformly ^{15}N-enriched PhPc was produced without the leader peptide and purified as described[53] with the following modifications: after cell lysis and ultracentrifugation, the supernatant was dialyzed against 0.5 mM ZnCl$_2$ and 5 mM Tris·HCl, pH 7.5

overnight at 4 °C. Pc concentrations were determined using $\varepsilon_{280} = 5.00$ cm^{-1} mM^{-1} on a Cary 50 spectrophotometer (Varian). The yield of pure protein was 3.5 mg L^{-1} of culture for ^{15}N-PhPc.

NMR measurements: All Pcs were concentrated by ultrafiltration (Amicon, M_w-cutoff 3 kDa). The sample buffer was 10 mM sodium phosphate, pH 6.5, and 6% D$_2$O. For peptide titrations, the protein concentrations were 200 μM for ^{15}N-DPc(Zn) and ^{15}N-PhPc(Zn) and 110 μM for ^{15}N-PoPc(Zn). The samples for fern Pc and poplar Pc backbone assignments consisted of 2.4 mM and 0.25 mM ^{13}C/^{15}N-labeled protein, respectively. Peptide solutions were prepared in 10 mM sodium phosphate, pH 6.5. All NMR spectra were recorded at 300 K on a Bruker AVIII600 spectrometer equipped with a triple-resonance TXI-Z-GRAD cryoprobe, or a Bruker 600 MHz Avance DRX spectrometer equipped with a 5 mm TCI cryoprobe. Data were processed with TopSpin (Bruker) and analyzed in SPARKY.[55] Resonances in the HSQC spectra of DPc and PoPc were assigned using 3D HNCACB experiments. The side chain resonance assignments of PoPc were taken from PoPc(Cd).[32] NMR assignments have been deposited to the BMRB, entry codes 19236 (DPc) and 19247 (PoPc).

PRE analysis: The paramagnetic X-Lys$_4$ and Lys$_4$-X peptides were added into ^{15}N-labelled Pc separately, and ^{1}H,^{15}N HSQC spectra were recorded. Each paramagnetic peptide was added to Pc at a peptide/Pc molar ratio of 0.5 for DPc and 1 for PoPc and PhPc. Under these conditions, the fractions of bound Pc were 14% for DPc and 35% for PoPc. Diamagnetic spectra were recorded by reducing the peptides with sodium ascorbate (5 equiv). PREs were determined according to the procedure of Battiste and Wagner.[54] The intensity ratio (I_{para}/I_{dia}) of the Pc resonances in the presence of X-Lys$_4$ or Lys$_4$-X was normalized by dividing by the average value of the ten largest I_{para}/I_{dia} values. The scaling factors for each Pc–peptide were 0.92, 0.87, 0.93, 1.07, 0.94, and 0.95 for PoPc–Lys$_4$-X, PoPc–X-Lys$_4$, DPc–Lys$_4$-X, DPc–X-Lys$_4$, PhPc–KKKX and PhPc–X-Lys$_4$, respectively.

PRE (R_2^{para}) values were calculated according to Equation (1):

$$\frac{I_{para}}{I_{dia}} = \frac{R_2^{dia} \exp(-R_2^{para}t)}{R_2^{dia} + R_2^{para}} \tag{1}$$

The transverse relaxation rates in the diamagnetic sample (R_2^{dia}) were calculated from the line width at half height obtained from a Lorentzian peak fit in the direct dimension using SPARKY. The symbol t denotes the time for transverse relaxation during the pulse sequence (9 ms).

Calculation of dissociation constants: Peptide binding was observed through the changes of protein resonances in the ^{1}H,^{15}N HSQC spectrum upon titration with the peptide. CSP analysis was carried out as described before.[56] The dissociation constants (K_d) for PoPc were determined using a two-parameter nonlinear regression curve fitting based on a one-site binding model as described previously.[57] The fraction of bound ligand was calculated using the dissociation constant. For DPc, resonance overlap was observed for Thr79/Glu25 and Ala23/Phe12 during the titrations. These four residues were excluded from the K_d calculation. The peptide–DPc interaction was modeled with two independent binding sites (Scheme 1). P and L in-
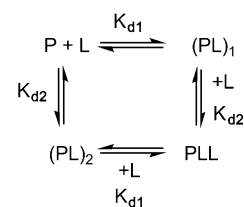
Scheme 1. Two-site binding model of DPc. P, protein; L, ligand; K_{d1} and K_{d2}, dissociation constants.

dicate the free protein and the free peptide, respectively. $(PL)_1$ and $(PL)_2$ are the 1:1 complexes formed by peptide binding to sites 1 and 2 on DPc, respectively. PLL is the protein with two peptides bound. K_{d1} and K_{d2} are the dissociation constants for sites 1 and 2, respectively. The binding curves were simulated numerically with varying values for K_{d1}, K_{d2}, and the $\Delta\delta$ at 100% bound Pc using Microsoft Excel.

Ensemble docking: For DPc, PhPc, and PoPc, the PDB IDs 1KDI,[7] 2Q5B, and Pc from 1TKW model 1[32] were used, respectively. The structure of Pc in 1TKW originated from PDB 5PCY.[4] The RMSD of all atoms between Pc in 1TKW and 5PCY is 0.15 Å.

The PREs were converted into distances for structure calculations as described previously.[56] τ_c was taken to be 5.54 ns for DPc, 5.14 ns for PoPc, and 5.93 ns for PhPc, on the basis of the HYDRONMR[58] prediction of the rotational correlation time for each Pc. For each peak, R_2 was estimated from the width at half-height ($\Delta\nu_{1/2}$) of a Lorentzian fit in the proton dimension by using $R_2 = \pi\Delta\nu_{1/2}$. PRE values were calculated after normalization of the I_{para}/I_{dia} ratios and extrapolated to 100% bound by dividing the values by their bound fractions (35% for PoPc and 14% for DPc). Three classes of PRE restraints were included in the calculations:[29] 1) For amide residues whose resonances disappear in the paramagnetic spectrum, an upper limit for I_{para} was estimated from the standard deviation of the noise level of the spectrum. The upper bound PRE (R_2^{para}) value was set to 500 s^{-1} and the distance set to 9 Å. 2) For residues with $I_{para}/I_{dia} > 0.85$, the lower bound distance was set to 15 Å. 3) For residues with I_{para}/I_{dia} between 0.1 and 0.85, the distances (r) calculated according to a previously described equation[56] were used, with upper and lower bounds of ($r \pm 0.1$) Å. Violations were defined as the absolute differences between the calculated distance and the experimental distance including the corresponding upper and lower bound margins for the three classes. An additional restraint ensures that the TOAC nitroxy oxygen atom and the Pc center of mass are at a distance between 10 and 30 Å. The structure calculations were done in XPLOR-NIH.[59] The accessible surface area (ASA) of each amide proton was calculated with a Python-based implementation of the Shrake–Rupley algorithm.[60]

Monte Carlo simulations: The peptide coordinates of X-Lys$_4$ and Lys$_4$-X were generated from the PRODRG server,[61] and the conformations were optimized in Swiss PDB-Viewer[62] to separate the charges as far as possible (Figure S6). For DPc, PhPc, and PoPc the PDB IDs 1KDI,[7] 2Q5B, and 1TKW model 1[32] were used, respectively. Structure preparation and the rigid-body MC simulation[37] were performed as described.[35,36] The electrostatic potential was calculated with APBS[63] for an ionic strength of 0.01 M and a temperature of 300 K to match the experimental conditions. An ensemble of 2000 peptide orientations, randomly selected from the entire run of 2.2×10^6 saved structures, was considered for the calculations. The averaged distances were derived from the ensemble and compared to the experimental distances.

Acknowledgements

[1] Q. Bashir, S. Scanu, M. Ubbink, *FEBS J.* **2011**, *278*, 1391–1400.
[2] M. Ubbink, *FEBS Lett.* **2009**, *583*, 1060–1066.
[3] G. McLendon, *Struct. Bonding (Berlin)* **1991**, *75*, 159–174.
[4] J. M. Guss, P. R. Harrowell, M. Murata, V. A. Norris, H. C. Freeman, *J. Mol. Biol.* **1986**, *192*, 361–387.
[5] J. M. Moore, C. A. Lepre, G. P. Gippert, W. J. Chazin, D. A. Case, P. E. Wright, *J. Mol. Biol.* **1991**, *221*, 533–555.
[6] C. S. Bond, D. S. Bendall, H. C. Freeman, J. M. Guss, C. J. Howe, M. J. Wagner, M. C. J. Wilce, *Acta Crystallogr. Sect. D Biol. Crystallogr.* **1999**, *55*, 414–421.
[7] T. Kohzuma, T. Inoue, F. Yoshizaki, Y. Sasakawa, K. Onodera, S. Nagatomo, T. Kitagawa, S. Uzawa, Y. Isobe, Y. Sugimura, M. Gotowda, Y. Kai, *J. Biol. Chem.* **1999**, *274*, 11817–11823.
[8] T. P. Garrett, D. J. Clingeleffer, J. M. Guss, S. J. Rogers, H. C. Freeman, *J. Biol. Chem.* **1984**, *259*, 2822–2825.
[9] H. Sugawara, T. Inoue, C. Li, M. Gotowda, T. Hibino, T. Takabe, Y. Kai, *J. Biochem.* **1999**, *125*, 899–903.
[10] Y. Xue, M. Ökvist, Ö. Hansson, S. Young, *Protein Sci.* **1998**, *7*, 2099–2105.
[11] S. Bagby, P. C. Driscoll, T. S. Harvey, H. A. O. Hill, *Biochemistry* **1994**, *33*, 6611–6622.
[12] P. M. Colman, H. C. Freeman, J. M. Guss, M. Murata, V. A. Norris, J. A. M. Ramshaw, M. P. Venkatappa, *Nature* **1978**, *272*, 319–324.
[13] C. A. Collyer, J. M. Guss, Y. Sugimura, F. Yoshizaki, H. C. Freeman, *J. Mol. Biol.* **1990**, *211*, 617–632.
[14] M. R. Redinbo, D. Cascio, M. K. Choukair, D. Rice, S. Merchant, T. O. Yeates, *Biochemistry* **1993**, *32*, 10560–10567.
[15] N. Shibata, T. Inoue, C. Nagano, N. Nishio, T. Kohzuma, K. Onodera, F. Yoshizaki, Y. Sugimura, Y. Kai, *J. Biol. Chem.* **1999**, *274*, 4225–4230.
[16] I. Bertini, D. A. Bryant, S. Ciurli, A. Dikiy, C. O. Fernández, C. Luchinat, N. Safarov, A. J. Vila, J. Zhao, *J. Biol. Chem.* **2001**, *276*, 47217–47226.
[17] L. Schmidt, H. E. M. Christensen, P. Harris, *Acta Crystallogr. Sect. D Biol. Crystallogr.* **2006**, *62*, 1022–1029.
[18] I. Díaz-Moreno, A. Díaz-Quintana, M. A. De La Rosa, M. Ubbink, *J. Biol. Chem.* **2005**, *280*, 18908–18915.
[19] R. Hulsker, M. V. Baranova, G. S. Bullerjahn, M. Ubbink, *J. Am. Chem. Soc.* **2008**, *130*, 1985–1991.
[20] S. Hirota, K. Hayamizu, M. Endo, T. Hibino, T. Takabe, T. Kohzuma, O. Yamauchi, *J. Am. Chem. Soc.* **1998**, *120*, 8177–8183.
[21] S. Hirota, M. Endo, T. Tsukazaki, *J. Biol. Inorg. Chem.* **1998**, *3*, 563–569.
[22] S. Hirota, M. Endo, *J. Am. Chem. Soc.* **1999**, *121*, 849–855.
[23] S. Hirota, K. Hayamizu, T. Okuno, M. Kishi, H. Iwasaki, T. Kondo, *Biochemistry* **2000**, *39*, 6357–6364.
[24] S. Hirota, T. Tsukazaki, O. Yamauchi, *Biochem. Biophys. Res. Commun.* **2000**, *268*, 395–397.
[25] S. Hirota, O. Yamauchi, *Eur. J. Inorg. Chem.* **2002**, 17–25.
[26] S. Hirota, O. Yamauchi, *Chem. Rec.* **2001**, *1*, 290–299.
[27] J. Iwahara, G. M. Clore, *Nature* **2006**, *440*, 1227–1230.
[28] G. M. Clore, J. Iwahara, *Chem. Rev.* **2009**, *109*, 4108–4139.
[29] H. E. Lindfors, P. E. de Koning, J. W. Drijfhout, B. Venezia, M. Ubbink, *J. Biomol. NMR* **2008**, *41*, 157–167.
[30] S. Schreier, J. C. Bozelli, N. Marín, R. F. F. Vieira, C. R. Nakaie, *Biophys. Rev.* **2012**, *4*, 45–66.
[31] R. Hulsker, A. Mery, E. A. Thomassen, A. Ranieri, M. Sola, M. P. Verbeet, T. Kohzuma, M. Ubbink, *J. Am. Chem. Soc.* **2007**, *129*, 4423–4429.
[32] C. Lange, T. Cornvik, I. Díaz-Moreno, M. Ubbink, *Biochim. Biophys. Acta Bioenerg.* **2005**, *1707*, 179–188.
[33] S. Hirota, H. Okumura, S. Arie, K. Tanaka, M. Shionoya, T. Takabe, N. Funasaki, Y. Watanabe, *J. Inorg. Biochem.* **2004**, *98*, 849–855.
[34] R. Hulsker, *PhD thesis*, Leiden University (The Netherlands), **2008**.
[35] S. Scanu, J. M. Foerster, G. M. Ullmann, M. Ubbink, *J. Am. Chem. Soc.* **2013**, *135*, 7681–7892.
[36] Q. Bashir, A. N. Volkov, G. M. Ullmann, M. Ubbink, *J. Am. Chem. Soc.* **2010**, *132*, 241–247.

[37] G. M. Ullmann, E. Knapp, N. M. Kostić, *J. Am. Chem. Soc.* **1997**, *119*, 42–52.

[38] R. K. Jain, A. D. Hamilton, *Org. Lett.* **2000**, *2*, 1721–1723.

[39] T. Aya, A. Hamilton, *Bioorg. Med. Chem. Lett.* **2003**, *13*, 2651–2654.

[40] P. B. Crowley, P. Ganji, H. Ibrahim, *ChemBioChem* **2008**, *9*, 1029–1033.

[41] Y. Wei, G. McLendon, A. D. Hamilton, *Chem. Commun.* **2001**, 1580–1581.

[42] R. E. McGovern, H. Fernandes, A. R. Khan, N. P. Power, P. B. Crowley, *Nat. Chem.* **2012**, *4*, 527–533.

[43] S. Fletcher, A. D. Hamilton, *Curr. Opin. Chem. Biol.* **2005**, *9*, 632–638.

[44] H. Yin, A. D. Hamilton, *Angew. Chem.* **2005**, *117*, 4200–4235; *Angew. Chem. Int. Ed.* **2005**, *44*, 4130–4163.

[45] S. Fletcher, A. D. Hamilton, *J. R. Soc. Interface* **2006**, *3*, 215–233.

[46] T. Mecca, G. Consoli, C. Geraci, F. Cunsolo, *Bioorg. Med. Chem.* **2004**, *12*, 5057–5062.

[47] M. Blaskovich, Q. Lin, F. Delarue, J. Sun, H. S. Park, D. Coppola, A. D. Hamilton, S. M. Sebti, *Nat. Biotechnol.* **2000**, *18*, 1065–1070.

[48] J. A. R. Worrall, Y. Liu, P. B. Crowley, J. M. Nocek, B. M. Hoffman, M. Ubbink, *Biochemistry* **2002**, *41*, 11721–11730.

[49] X. Xu, W. Reinle, F. Hannemann, P. V. Konarev, D. I. Svergun, R. Bernhardt, M. Ubbink, *J. Am. Chem. Soc.* **2008**, *130*, 6395–6403.

[50] M. Ubbink, D. S. Bendall, *Biochemistry* **1997**, *36*, 6326–6335.

[51] A. N. Volkov, D. Ferrari, J. A. R. Worrall, A. M. J. J. Bonvin, M. Ubbink, *Protein Sci.* **2005**, *14*, 799–811.

[52] M. Cai, Y. Huang, K. Sakaguchi, G. M. Clore, A. M. Gronenborn, R. Craigie, *J. Biomol. NMR* **1998**, *11*, 97–102.

[53] P. B. Crowley, G. Otting, B. G. Schlarb-Ridley, G. W. Canters, M. Ubbink, *J. Am. Chem. Soc.* **2001**, *123*, 10444–10453.

[54] J. L. Battiste, G. Wagner, *Biochemistry* **2000**, *39*, 5355–5365.

[55] T. D. Goddard, D. G. Kneller, SPARKY 3.0, University of California, San Francisco, **2008**.

[56] S. Scanu, J. M. Foerster, M. G. Finiguerra, M. H. Shabestari, M. Huber, M. Ubbink, *ChemBioChem* **2012**, *13*, 1312–1328.

[57] A. Kannt, S. Young, D. S. Bendall, *Biochim. Biophys. Acta Bioenerg.* **1996**, *1277*, 115–126.

[58] J. García de La Torre, M. L. Huertas, B. Carrasco, *J. Magn. Reson.* **2000**, *147*, 138–146.

[59] C. D. Schwieters, J. J. Kuszewski, N. Tjandra, G. M. Clore, *J. Magn. Reson.* **2003**, *160*, 65–73.

[60] A. Shrake, J. A. Rupley, *J. Mol. Biol.* **1973**, *79*, 351–371.

[61] A. W. Schüttelkopf, D. M. F. van Aalten, *Acta Crystallogr. Sect. D Biol. Crystallogr.* **2004**, *60*, 1355–1363.

[62] N. Guex, M. C. Peitsch, *Electrophoresis* **1997**, *18*, 2714–2723.

[63] N. A. Baker, D. Sept, S. Joseph, M. J. Holst, J. A. McCammon, *Proc. Natl. Acad. Sci. USA* **2001**, *98*, 10037–10041.

[64] The PyMOL Molecular Graphics System, Version 0.99, Schrödinger, LLC.